Applied Physics Letters

Creation of single chiral soliton states in monoaxial helimagnets

Cite as: Appl. Phys. Lett. **119**, 222405 (2021); https://doi.org/10.1063/5.0067682
Submitted: 18 August 2021 • Accepted: 16 November 2021 • Published Online: 02 December 2021

S. A. Osorio, V. Laliena, J. Campo, et al.

Applied Physics Letters ARTICLE scitation.org/journal/apl

Creation of single chiral soliton states in monoaxial helimagnets

Cite as: Appl. Phys. Lett. **119**, 222405 (2021); doi: 10.1063/5.0067682
Submitted: 18 August 2021 · Accepted: 16 November 2021 ·
Published Online: 2 December 2021

S. A. Osorio,[1] V. Laliena,[2] J. Campo,[3] and S. Bustingorry[1,a)]

AFFILIATIONS

[1]Instituto de Nanociencia y Nanotecnología, CNEA-CONICET, Centro Atómico Bariloche, Av. E. Bustillo 9500, R8402AGP San Carlos de Bariloche, Río Negro, Argentina
[2]Department of Applied Mathematics, University of Zaragoza, C/María de Luna 3, 50018 Zaragoza, Spain
[3]Aragon Nanoscience and Materials Institute (CSIC—University of Zaragoza) and Condensed Matter Physics Department, University of Zaragoza, C/Pedro Cerbuna 12, 50009 Zaragoza, Spain

[a)]Author to whom correspondence should be addressed: sbusting@cab.cnea.gov.ar

ABSTRACT

In monoaxial helimagnets, the Dzyaloshinskii–Moriya interaction favors inhomogeneous distributions of the magnetization with chiral modulations of solitonic character. In addition to the helical magnetic state at zero field, a chiral soliton lattice can be stabilized when a magnetic field perpendicular to the chiral axis is applied. When the magnetic field is increased, the system undergoes a phase transition to the uniform state at a critical field B_c. Above B_c, a single chiral soliton comprises the lowest level excitation over the stable uniform state, surviving as a metastable configuration. How to retain a single chiral soliton metastable state has not been addressed yet. Using micromagnetic simulations, we analyze this possibility by injecting spin polarized currents and put forward a feasible protocol to obtain a state with a single chiral soliton from the chiral soliton lattice. Our proposal could be relevant in the experimental study of metastable solitons for technological applications.

Topology and chirality are the principal avenues along which the field of spintronics currently transits.[1] While topology is usually related to the presence of robust states against continuous or weak fluctuations, chirality refers to the handedness of a state that are commonly encountered in systems whose inversion symmetry is broken. Both, topological and chiral features, meet together in magnetic systems where the antisymmetric Dzyaloshinskii–Moriya interaction (DMI) plays a key role.[2,3] This interaction emerges due to the space inversion symmetry breaking and is the responsible for the stabilization of solitonic configurations. Among them, the skyrmion is a prominent representative and many important properties and functionalities were found to be attached to the topologically nontrivial skyrmionic texture, such as emergent electromagnetic fields, low depinning currents, and small size.[1,4–6] From data storage to information transmission and processing,[7–12] the spectrum of potential applications is a growing field since its experimental discovery in the chiral ferromagnet MnSi.[13]

Another interesting topological object emerges in monoaxial chiral helimagnets, a subclass of chiral magnets in which the DMI acts along a specific direction (chiral axis) determined by the symmetry of the underlying crystalline lattice. Besides the archetypal $CrNb_3S_6$, the list of monoaxial helimagnets includes a wide range of magnetic compounds, such as $CrTa_3S_6$, CuB_2O_4, $CuCsCl_3$, $Yb(Ni_{1-x}Cu_x)_3Al_9$, and $Ba_2CuGe_2O_7$.[14–20] All these systems share similar magnetic properties and, remarkably, they feature chiral modulations of the magnetization field. Besides the zero field helical state (HL), a chiral soliton lattice (CSL) state can be stabilized at finite magnetic field perpendicular to the chiral axis.[21–26] Furthermore, single chiral solitonic magnetic structures of topological nature are found as metastable states in monoaxial helimagnets.[27] These objects have many interesting properties for potential applications in spintronic devices, showing advantages over domain walls, which are severely affected by pinning effects, which difficult domain wall motion,[28–30] and over skyrmions, whose external control is hindered by gyrotropic effects.[4,31,32]

The magnetic phase diagram has been extensively studied from the experimental and theoretical points of view, providing a clear picture of the field and temperature characteristics of the phase transitions among stable phases.[33–47] In contrast, the metastability of chiral magnetic textures has received less attention. In particular, the metastability of single chiral solitons (CSs) has recently been studied in

Ref. 27, where the authors deduced the metastability phase diagram of a single CS through analytical methods.

In this article, we numerically investigate how to control the number CSs in a chiral helimagnet through the injection of spin currents. Furthermore, we detail a proposal to obtain a metastable single CS state from the CSL, which provides a feasible experimental setup for future spintronic devices.

The dynamical evolution of the magnetization field in a ferromagnet under current induced external torque is governed by the modified Landau–Lifshitz–Gilbert (LLG) equation:

$$\frac{\partial \mathbf{n}}{\partial t} = \gamma \mathbf{B}_{eff} \times \mathbf{n} + \alpha \mathbf{n} \times \left(\frac{\partial \mathbf{n}}{\partial t}\right) + \boldsymbol{\tau}, \tag{1}$$

where α and γ are the Gilbert damping and the gyromagnetic constant, respectively. The vector field $\mathbf{B}_{eff}(\mathbf{r}) = -\frac{1}{M_S}\frac{\delta E}{\delta \mathbf{n}(\mathbf{r})}$ is the effective field derived from the energy functional E. The unimodular vector field $\mathbf{n}(\mathbf{r}) = \mathbf{M}(\mathbf{r})/M_S$ describes the local magnetization direction, and M_S is the saturation magnetization. The last term in Eq. (1), $\boldsymbol{\tau}$, is the external torque due to the spin-polarized current, and it is given by

$$\boldsymbol{\tau} = -b_j(\mathbf{j}\cdot\nabla)\mathbf{n} + \beta b_j \mathbf{n} \times (\mathbf{j}\cdot\nabla)\mathbf{n}, \tag{2}$$

where $b_j = \frac{P\mu_B}{eM_S}$, where P is the polarization degree, e is the electron charge, and μ_B is the Bohr magneton. The first term is the reactive (adiabatic) torque, and the second term is the dissipative (nonadiabatic) torque, whose strength is controlled by the nonadiabaticity coefficient β.[48,49]

The models describing a monoaxial chiral ferromagnet include ferromagnetic exchange interactions, monoaxial DMIs, and single-ion anisotropies, characterized by the stiffness constant A, the DMI strength constant D, and the anisotropy constant K, respectively. Thus, the magnetic energy functional is $E[e(r)] = \int d^3\mathbf{r} e(r)$, and the energy density $e(r)$ is given by

$$e(r) = A\sum_{i=x,y,z}(\partial_i \mathbf{n}\cdot\partial_i\mathbf{n}) - D\hat{\mathbf{z}}\cdot(\mathbf{n}\times\partial_z\mathbf{n}) - Kn_z^2 - M_S\mathbf{B}\cdot\mathbf{n}, \tag{3}$$

where the chiral axis is along $\hat{\mathbf{z}}$ and $\mathbf{B}$ is the external magnetic field. Henceforth, we consider a magnetic field perpendicular to the chiral axis and along the $\hat{\mathbf{y}}$ direction, $\mathbf{B} = B\hat{\mathbf{y}}$. The corresponding effective field in Eq. (1) reads

$$\mathbf{B}_{eff} = \frac{2}{M_S}\left[A\nabla^2\mathbf{n} - D\hat{\mathbf{z}}\times\partial_z\mathbf{n} + K\hat{\mathbf{z}}(\hat{\mathbf{z}}\cdot\mathbf{n}) + \frac{M_S B}{2}\hat{\mathbf{y}}\right]. \tag{4}$$

This model applies to a wide range of monoaxial helimagnets; thus, without losing generality, we chose $A = 1.42\,\mathrm{pJ/m}$, $D = 369\,\mu\mathrm{J/m^2}$, $K = -124\,\mathrm{kJ/m^3}$, and $M_S = 129\,\mathrm{kA/m}$, which is a suitable set of parameters to model the $CrNb_3S_6$ compound.[27] The effects of the dipolar interaction are effectively taken into account in the uniaxial anisotropy term. This approximation is exact for a magnetization field depending only on the z coordinate as occurs in an infinitely large system in the xy plane,[50] and it also holds for a system with periodic boundary conditions along the z coordinate provided that the spatial average of n_z vanishes, $\langle n_z\rangle = 0$, a condition approximately fulfilled in our simulations (see supplementary material note 1). Dipolar surface effects can be neglected since the typical length scales are larger than $A/K_S \approx 10\,\mathrm{nm}$, with K_S the surface anisotropy. We neglect thermal effects working at zero temperature, which provides reliable results for finite temperatures well below the Curie temperature T_c.

Our numerical studies and results are found on the basis of micromagnetic simulations using the MuMax3 numerical code, which provides an efficient environment for the integration of the LLG equation in a vast variety of conditions.[51,52] In dealing with monoaxial helimagnets, the introduction of the DMI must be properly addressed. For this purpose, we have adapted the conventional DMI package in order to account for this monoaxial character.[27,53] Our implementation for the DMI correctly describes the behavior of the $CrNb_3S_6$ compound;[21–24,54] namely, it exhibits a helical state (HL) at zero magnetic field and a CSL (comprised of a periodic array of CSs) for finite magnetic fields [see Fig. 1(a)] up to the saturation field $B_c \approx 228\,\mathrm{mT}$ [see supplementary material note 2, Fig. S1(a)]. Furthermore, effects associated with the transitions between different topological sectors in finite size systems[55–57] are well described by our simulations as shown in supplementary material note 2 and Figs. S1(b)–S1(d). In this case, the number of CSs in the ground state decreases with the magnetic field.[58] Furthermore, for a system of length $L_z = 500\,\mathrm{nm}$, we present in

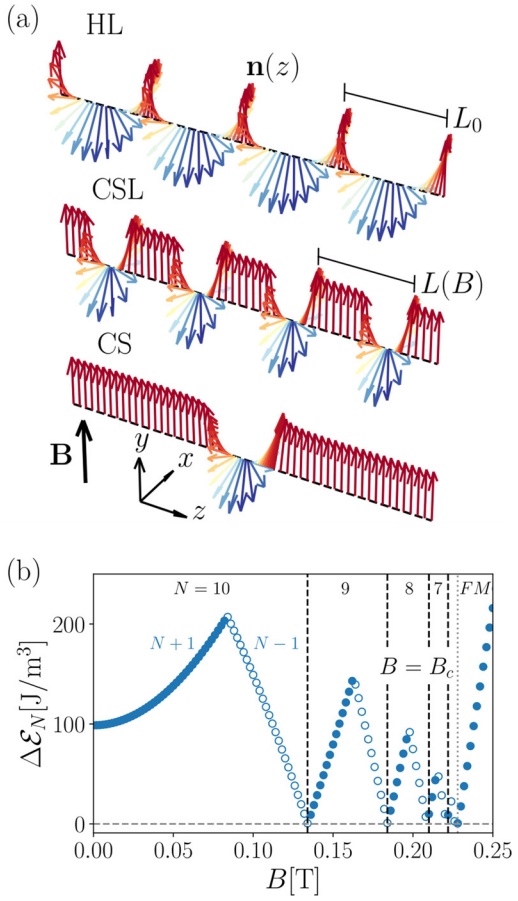

FIG. 1. (a) A representation of helical (HL), chiral soliton lattice (CSL), and single chiral soliton (CS) states. (b) Difference in energy between the stable state and the first metastable state. If the stable state contains N solitons, the first metastable state might comprise $N+1$ (closed circles) or $N-1$ (open circles) solitons. For $B > B_c$, the single CS is the first metastable state.

Fig. 1(b) the difference in energy between the stable state and the first metastable state $\Delta E_N = \min\{E_{N+1} - E_N, E_{N-1} - E_N\}$, with N the corresponding number of solitons at a given value of B. This shows that while the first metastable state contains $N+1$ or $N-1$ CSs below B_c, for $B > B_c$ the single CS is the first metastable state.

At this point, it is extremely important to analyze the stability limits of the CS state. This permits us to fix the range of magnetic fields (perpendicular to the chiral axis) where the CS state can be created and retained. Indeed, we have shown, using micromagnetic simulations, that the single CS state can be metastably found in a wide range of magnetic fields, $0 < B < B_z^* \approx 1490$ mT (see supplementary material note 3). This result is in excellent agreement with that obtained analytically $B_z^* \approx 1493$ mT.[27]

Since the CSL is the stable state at finite but low magnetic field, we can take this many-soliton state as the starting condition to create a single CS state. In principle, this could be achieved by tuning the magnetic field in a narrow region below and very close to B_c. The fact that the number of CSs varies dramatically in this region makes the control of this process a difficult task. It has been shown that soliton nucleation can be controlled by applying dynamic strain.[59] Instead, we propose to use a spin-polarized current applied to the CSL to finally reach a state with a single CS. Although the topological character of the CSs and the repulsive interaction between them prevent their decay and collapse into the trivial FM state, when pushed against each other it is possible to destroy the solitons one-by-one if the driving force is strong enough.

We consider the setup schematically shown in the inset of Fig. 2(b) in which the current has opposite directions on each half of the system. This setup was originally studied by Koumpouras *et al.*,[60] where the authors showed that in a two-soliton line the destruction of a CS occurs when they are pushed against each other. To analyze this phenomenology, we perform micromagnetic simulations on a system of size $L_x \times L_y \times L_z = 1 \times 1 \times 500\,\text{nm}^3$, discretized in cubic cells of volume 1nm^3 with periodic boundary conditions. Taking as the initial configuration a random perturbation around an homogeneous magnetic configuration along the chiral axis, the system is let to relax at a fixed magnetic field $B = 10$ mT, resulting in a metastable state corresponding to a CSL with $N = 13$ magnetization rotations (2π rotations around the chiral axis). We chose $P = 1$, $\alpha = 0.01$, and $\beta = 0.02$ for the polarization degree, the Gilbert damping, and the nonadiabaticity constant, respectively. The strength of the current density grows linearly with the time from $j = 0$ A/m^2 up to $j_{max} = 2.75 \times 10^{12}$ A/m^2 as shown in Fig. 2(a) (see supplementary material note 4).

In Fig. 2(b), we show (in red) the evolution of the energy density during the application of the current protocol. When the current density ramp is applied the energy density first increases, showing a sudden

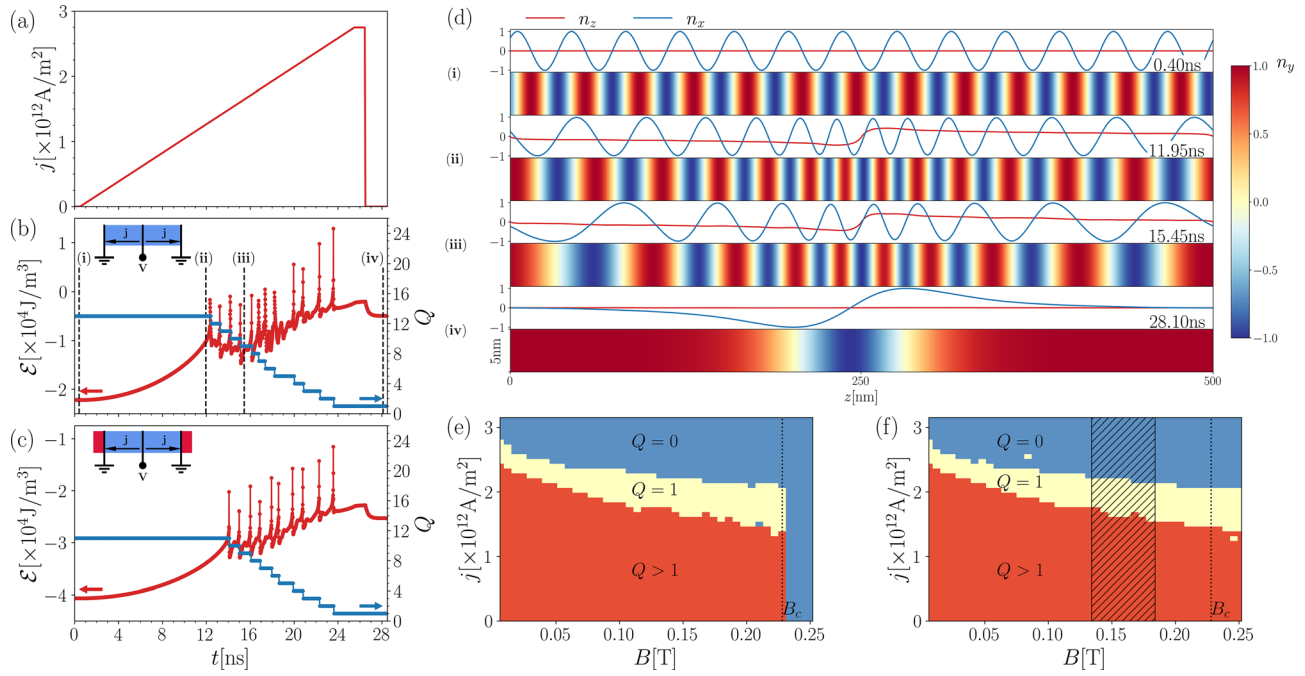

FIG. 2. Destruction of CSs by opposing currents. (a) Current density as a function of time. Energy density (red) and winding number (blue) as a function of time for the system with periodic boundary conditions (b) and for the system with engineered edges (c). The insets of (b) and (c) show the corresponding setups. In (d), snapshots of the magnetization field at selected times are shown [as indicated in (b)] for the system with periodic boundary conditions: (i) initial state with 13 solitons before the current is applied, (ii) state with 13 solitons after the current is applied, (iii) state after the destruction of four CS, and (iv) final state, in which a single soliton remains, after the current is turned off. In (b)–(d), the magnetic field is $B = 10$ mT. (e)–(f) Phase diagrams in the $j - B$ space for a system with engineered edges, obtained by applying a 20 ns square current density pulse of intensity j to (e) the equilibrium state, whose number of solitons depends on B, and (f) to a metastable initial state with $N = 9$ solitons. The red, yellow, and blue regions correspond to final states, which contain more than one soliton ($Q > 1$), exactly one soliton ($Q = 1$), and no soliton ($Q = 0$), respectively. In the hatched region, the initial state is the equilibrium state, which contains $N = 9$ solitons.

drop around $t = 12.5$ ns. After this ($12.5 < t < 26.5$ ns), we recognize a series of cusps. In the final stretch ($t > 26.5$ ns), when the current density reaches it maximum value and then drops to zero, we see two subsequent plateaus. The cusps in the energy density are accompanied by the destruction of one CS at a time. This can be seen directly from the magnetization configuration, and we can quantify the number of CSs through the winding number $Q = \sum_i \{\arcsin[(\mathbf{n}_{\perp,i} \times \mathbf{n}_{\perp,i+1}) \cdot \hat{\mathbf{z}}]\}$, where the sum runs over the number of cells along the chiral axis and $\hat{\mathbf{z}} \cdot \mathbf{n}_{\perp,i} = 0$. This quantity measures the number of times the $\mathbf{n}_\perp$ component winds around the chiral axis, and therefore, it is a measure of the number of solitons in the system. As shown in Fig. 2(b) (in blue), concomitantly with the cusps in the energy density, Q decreases in unitary steps, as a result of the destruction of one soliton in the system. At $t \sim 24$ ns, the system ends up with one CS ($Q = 1$) localized at the center whose width is $\Delta = 80$ nm when the current is turned off [see Fig. 2(d)-iv], which is consistent with the expected width $\Delta = 83$ nm from analytical results.[27] The modulation of the CS train varies with the position along the chiral axis when the current is applied, being longer at the opposite extremes and shorter at the center of the system as shown in Figs. 2(d)-(i)–2(d)-(iii) for the transition from $N = 13$ to $N = 9$. The destruction process of a single soliton involves strong variations of the magnetization field in the center of the system, in particular in the n_z component (see supplementary material note 4).

Since our previous simulations were carried out using periodic boundary conditions, it is natural to ask if our results are still valid for system of finite size with open boundary conditions along the chiral axis (and periodic boundary conditions along the other two directions), an even more realistic situation. It is well known that in this case, the DMI induces non-trivial boundary conditions.[53,61] The most important consequence of these boundary conditions is that the DMI induces a spatial rearrangement of $\mathbf{n}$ along the chiral axis at the ends of the sample, known as chiral twists.[61–65] The scale of these rearrangements is characterized by the ratio A/D. These chiral twists, which are relevant to the present work since they are due to the surface energy barriers governing the CSs penetration from the edges,[45,46,66] are automatically taken into account by the implementation of open boundary conditions. However, a detailed discussion of chiral twists is outside the scope of this work. Under the action of the torque due to the spin-polarized current, the creation of CSs at the boundary of the system is promoted, which subsequently move to the center of the sample. Though the destruction process is still present at the center of the sample, the creation of solitons occurs simultaneously and the number of solitons does not decrease when an electrical pulse is applied (see supplementary material note 5). Thus, the concept discussed previously turns out to be inefficient for the open system. In order to circumvent this problem, we induce a strong easy-axis anisotropy at both ends of the sample. The easy-axis should be perpendicular to the chiral axis. The relevance of the easy-axis at both ends of the sample is twofold. First, it strongly confines the solitonic states inside a finite region (see Ref. 58). Second, and more important, the strong boundary conditions imposed by these easy-axis inhibit the surface induced creation of CSs that would otherwise occur in the open system.

We then consider an open system with engineered edges, i.e., with both ends of the system properly designed to have different magnetic properties. At both ends of the system, we put a hard ferromagnet modeled by two pieces of 50 nm long with parameters $A' = A$ and $K' = |K|$, for the stiffness constant and the uniaxial anisotropy (easy-axis along $\hat{\mathbf{y}}$), respectively. In between, we insert a 500 nm long chiral magnet as considered previously. With these improvements, the open system behaves in the same way as that with periodic boundary conditions [see Fig. 2(c) and supplementary material note 6]. Thus, through the procedure of the previous discussion, we can obtain a metastable state with any number of solitons fixed by the final value of the current density ramp. Therefore, we might conceive that a desired state with fixed number of solitons can be reached by applying a square current pulse of the appropriate time duration and current density intensity. Figures 2(b), 2(c), and S5(b) show that the energy relaxation following the cusp is fast, for both the system with periodic or with engineered edges, and then we set the time duration of the current pulse to 20 ns.

It is very interesting to study the number of solitons remaining in the final state as a function of the current intensity. To this end, we apply a 20 ns square current pulse and compute the number of CSs in the final state, after the current has been removed. The result is shown in Fig. 2(e) for the system with engineered edges and the equilibrium state as initial condition, when $j = 0\,\mathrm{A/m^2}$. The figure shows the regions on the $j - B$ space where the final state contains more than one soliton (red), exactly one soliton (yellow), and no soliton (blue). We notice that the final state contains exactly one soliton in a wide region of the $j - B$ phase diagram, which is very important since it means that it is not necessary to fine-tune the current intensity or the pulse duration to end up with a single soliton. The same plot is shown in Fig. 2(f) for the case in which the initial condition is a state with $N = 9$ solitons, which is the equilibrium state only in the hatched region. The figure is very similar to Fig. 2(e), which proves that the final state topology is basically independent of the initial state, and depends only on the intensity of the applied current (see supplementary material note 7).

Summarizing, we propose the following strategy to obtain a single soliton metastable state in a monoaxial helimagnet: Considering a sample with edges engineered so that a strong easy-axis anisotropy appears at the edges, apply a low magnetic field, so that the equilibrium state is a CSL, and inject a pulse of opposed currents from the center of the sample. The solitons from both sides of the sample move toward the center, where they are destroyed one-by-one until exactly one remains. Afterward, the pulse current is removed and the single soliton state survives as a metastable state. If desired, the applied field can be slowly increased beyond the critical field, where the equilibrium state is FM and the single soliton state is still metastable. Remarkably, this strategy exhibits a strong robustness against the magnetization distribution in the initial state. In light of this, our results show that the proposed protocol to obtain single CSs is a promising setup for experimentally testing their metastability.

See the supplementary material for details on the validation of the micromagnetic simulations and for the results of additional micromagnetic simulations on the chiral soliton metastability and creation.

The authors thank J. Curiale and L. Avilés-Félix for the enlightening and fruitful discussions. This work was supported by Grant No. PGC2018099024B100 funded by MCIN/AEI/10.13039/501100011033. Grants OTR02223 from CSIC/MICIN and DGA-M4 from Diputación General de Aragón, Spain, are also acknowledged. This work was also supported by the Grant No.

PICT 2017-0906 from the Agencia Nacional de Promoción Científica y Tecnológica, Argentina.

AUTHOR DECLARATIONS

Conflict of Interest

The authors have no conflicts to disclose.

DATA AVAILABILITY

The data that support the findings of this study are available from the corresponding author upon reasonable request.

REFERENCES

[1]C. Back, V. Cros, H. Ebert, K. Everschor-Sitte, A. Fert, M. Garst, T. Ma, S. Mankovsky, T. L. Monchesky, M. Mostovoy, N. Nagaosa, S. S. P. Parkin, C. Pfleiderer, N. Reyren, A. Rosch, Y. Taguchi, Y. Tokura, K. von Bergmann, and J. Zang, "The 2020 skyrmionics roadmap," J. Phys. D **53**, 363001 (2020).

[2]I. Dzyaloshinsky, "A thermodynamic theory of 'weak' ferromagnetism of antiferromagnetics," J. Phys. Chem. Solids **4**, 241–255 (1958).

[3]T. Moriya, "New mechanism of anisotropic superexchange interaction," Phys. Rev. Lett. **4**, 228 (1960).

[4]N. Nagaosa and Y. Tokura, "Topological properties and dynamics of magnetic skyrmions," Nat. Nanotechnol. **8**, 899 (2013).

[5]X. Yu, N. Kanazawa, W. Zhang, T. Nagai, T. Hara, K. Kimoto, Y. Matsui, Y. Onose, and Y. Tokura, "Skyrmion flow near room temperature in an ultralow current density," Nat. Commun. **3**, 988 (2012).

[6]T. Schulz, R. Ritz, A. Bauer, M. Halder, M. Wagner, C. Franz, C. Pfleiderer, K. Everschor, M. Garst, and A. Rosch, "Emergent electrodynamics of skyrmions in a chiral magnet," Nat. Phys. **8**, 301–304 (2012).

[7]J. Sampaio, V. Cros, S. Rohart, A. Thiaville, and A. Fert, "Nucleation, stability and current-induced motion of isolated magnetic skyrmions in nanostructures," Nat. Nanotechnol. **8**, 839 (2013).

[8]R. Tomasello, E. Martinez, R. Zivieri, L. Torres, M. Carpentieri, and G. Finocchio, "A strategy for the design of skyrmion racetrack memories," Sci. Rep. **4**, 6784 (2014).

[9]A. Fert, V. Cros, and J. Sampaio, "Skyrmions on the track," Nat. Nanotechnol. **8**, 152–156 (2013).

[10]X. Zhang, M. Ezawa, D. Xiao, G. Zhao, Y. Liu, and Y. Zhou, "All-magnetic control of skyrmions in nanowires by a spin wave," Nanotechnology **26**, 225701 (2015).

[11]Y. Zhou and M. Ezawa, "A reversible conversion between a skyrmion and a domain-wall pair in a junction geometry," Nat. Commun. **5**, 4652 (2014).

[12]X. Zhang, M. Ezawa, and Y. Zhou, "Magnetic skyrmion logic gates: Conversion, duplication and merging of skyrmions," Sci. Rep. **5**, 9400 (2015).

[13]S. Mühlbauer, B. Binz, F. Jonietz, C. Pfleiderer, A. Rosch, A. Neubauer, R. Georgii, and P. Böni, "Skyrmion lattice in a chiral magnet," Science **323**, 915–919 (2009).

[14]T. Moriya and T. Miyadai, "Evidence for the helical spin structure due to antisymmetric exchange interaction in $Cr_{1/3}NbS_2$," Solid State Commun. **42**, 209 (1982).

[15]Y. Kousaka, T. Ogura, J. Zhang, P. Miao, S. Lee, S. Torii, T. Kamiyama, J. Campo, K. Inoue, and J. Akimitsu, "Long periodic helimagnetic ordering in CrM_3S_6 (M = Nb and Ta)," J. Phys.: Conf. Ser. **746**, 012061 (2016).

[16]B. Roessli, J. Schäfer, G. A. Petrakovskii, B. Ouladdiaf, M. Boehm, U. Staub, A. Vorotinov, and L. Bezmaternikh, "Formation of a magnetic soliton lattice in copper metaborate," Phys. Rev. Lett. **86**, 1885–1888 (2001).

[17]K. Adachi, N. Achiwa, and M. Mekata, "Helical magnetic structure in $CsCuCl_3$," J. Phys. Soc. Jpn. **49**, 545–553 (1980).

[18]S. Ohara, S. Fukuta, K. Ohta, H. Kono, T. Yamashita, Y. Matsumoto, and J. Yamaura, "Study of chiral structure and magnetism in heavy-fermion $Yb(Ni_{1-x}Cu_x)_3Al_9$," JPS Conf. Proc. **3**, 017016 (2014).

[19]T. Matsumura, Y. Kita, K. Kubo, Y. Yoshikawa, S. Michimura, T. Inami, Y. Kousaka, K. Inoue, and S. Ohara, "Chiral soliton lattice formation in monoaxial helimagnet $Yb(Ni_{1-x}Cu_x)_3Al_9$," J. Phys. Soc. Jpn. **86**, 124702 (2017).

[20]A. Zheludev, S. Maslov, G. Shirane, Y. Sasago, N. Koide, and K. Uchinokura, "Field-induced commensurate-incommensurate phase transition in a Dzyaloshinskii-Moriya spiral antiferromagnet," Phys. Rev. Lett. **78**, 4857–4860 (1997).

[21]I. Dzyaloshinskii, "Theory of helicoidal structures in antiferromagnets. I. Nonmetals," Sov. Phys. JETP **19**, 960–971 (1964).

[22]T. Miyadai, K. Kikuchi, H. Kondo, S. Sakka, M. Arai, and Y. Ishikawa, "Magnetic properties of $Cr_{1/3}NbS_2$," J. Phys. Soc. Jpn. **52**, 1394 (1983).

[23]Y. A. Izyumov, "Modulated, or long-periodic, magnetic structures of crystals," Sov. Phys. Usp. **27**, 845 (1984).

[24]Y. Togawa, T. Koyama, K. Takayanagi, S. Mori, Y. Kousaka, J. Akimitsu, S. Nishihara, K. Inoue, A. Ovchinnikov, and J. Kishine, "Chiral magnetic soliton lattice on a chiral helimagnet," Phys. Rev. Lett. **108**, 107202 (2012).

[25]J. Kishine and A. Ovchinnikov, "Theory of monoaxial chiral helimagnet," Solid State Phys. **66**, 1–130 (2015).

[26]Y. Togawa, Y. Kousaka, K. Inoue, and J. Kishine, "Symmetry, structure, and dynamics of monoaxial chiral magnets," J. Phys. Soc. Jpn. **85**, 112001 (2016).

[27]V. Laliena, S. Bustingorry, and J. Campo, "Dynamics of chiral solitons driven by polarized currents in monoaxial helimagnets," Sci. Rep. **10**, 20430 (2020).

[28]S.-H. Yang, K.-S. Ryu, and S. Parkin, "Domain-wall velocities of up to 750 m s^{-1} driven by exchange-coupling torque in synthetic antiferromagnets," Nat. Nanotechnol. **10**, 221 (2015).

[29]V. Jeudy, R. Díaz Pardo, W. Savero Torres, S. Bustingorry, and A. B. Kolton, "Pinning of domain walls in thin ferromagnetic films," Phys. Rev. B **98**, 054406 (2018).

[30]L. Herrera Diez, M. Voto, A. Casiraghi, M. Belmeguenai, Y. Roussigné, G. Durin, A. Lamperti, R. Mantovan, V. Sluka, V. Jeudy, Y. T. Liu, A. Stashkevich, S. M. Chérif, J. Langer, B. Ocker, L. Lopez-Diaz, and D. Ravelosona, "Enhancement of the Dzyaloshinskii-Moriya interaction and domain wall velocity through interface intermixing in Ta/CoFeB/MgO," Phys. Rev. B **99**, 054431 (2019).

[31]W. Jiang, X. Zhang, G. Yu, W. Zhang, X. Wang, M. B. Jungfleisch, J. E. Pearson, X. Cheng, O. Heinonen, K. L. Wang, Y. Zhou, A. Hoffmann, and S. G. E. te Velthuis, "Direct observation of the skyrmion hall effect," Nat. Phys. **13**, 162 (2017).

[32]Y. Zhou, R. Mansell, and S. van Dijken, "Driven gyrotropic skyrmion motion through steps in magnetic anisotropy," Sci. Rep. **9**, 6525 (2019).

[33]Y. Togawa, Y. Kousaka, S. Nishihara, K. Inoue, J. Akimitsu, A. Ovchinnikov, and J. Kishine, "Interlayer magnetoresistance due to chiral soliton lattice formation in hexagonal chiral magnet $CrNb_3S_6$," Phys. Rev. Lett. **111**, 197204 (2013).

[34]N. Ghimire, M. A. McGuire, D. S. Parker, B. Sipos, S. Tang, J.-Q. Yan, B. C. Sales, and D. Mandrus, "Magnetic phase transition in single crystals of the chiral helimagnet $Cr_{1/3}NbS_2$," Phys. Rev. B **87**, 104403 (2013).

[35]K. Tsuruta, M. Mito, H. Deguchi, J. Kishine, Y. Kousaka, J. Akimitsu, and K. Inoue, "Phase diagram of the chiral magnet $Cr_{1/3}NbS_2$ in a magnetic field," Phys. Rev. B **93**, 104402 (2016).

[36]H. Han, L. Zhang, D. Sapkota, N. Hao, L. Ling, H. Du, L. Pi, C. Zhang, D. G. Mandrus, and Y. Zhang, "Tricritical point and phase diagram based on critical scaling in the monoaxial chiral helimagnet $Cr_{1/3}NbS_2$," Phys. Rev. B **96**, 094439 (2017).

[37]J. Yonemura, Y. Shimamoto, T. Kida, D. Yoshizawa, Y. Kousaka, S. Nishihara, F. J. T. Goncalves, J. Akimitsu, K. Inoue, M. Hagiwara, and Y. Togawa, "Magnetic solitons and magnetic phase diagram of the hexagonal chiral crystal $CrNb_3S_6$ in oblique magnetic fields," Phys. Rev. B **96**, 184423 (2017).

[38]E. M. Clements, R. Das, L. Li, P. J. Lampen-Kelley, M.-H. Phan, V. Keppens, D. Mandrus, and H. Srikanth, "Critical behavior and macroscopic phase diagram of the monoaxial chiral helimagnet $Cr_{1/3}NbS_2$," Sci. Rep. **7**, 6545 (2017).

[39]R. Aoki, Y. Kousaka, and Y. Togawa, "Anomalous nonreciprocal electrical transport on chiral magnetic order," Phys. Rev. Lett. **122**, 057206 (2019).

[40]T. Honda, Y. Yamasaki, H. Nakao, Y. Murakami, T. Ogura, Y. Kousaka, and J. Akimitsu, "Topological metastability supported by thermal fluctuation upon formation of chiral soliton lattice in $CrNb_3S_6$," Sci. Rep. **10**, 18596 (2020).

[41]Y. Nishikawa and K. Hukushima, "Phase transitions and ordering structures of a model of chiral helimagnet in three dimensions," Phys. Rev. B **94**, 064428 (2016).

[42]V. Laliena, J. Campo, and Y. Kousaka, "Understanding the H-T phase diagram of the monoaxial helimagnet," Phys. Rev. B **94**, 094439 (2016).
[43]M. Shinozaki, S. Hoshino, Y. Masaki, J. Kishine, and Y. Kato, "Finite-temperature properties of three-dimensional chiral helimagnets," J. Phys. Soc. Jpn. **85**, 074710 (2016).
[44]V. Laliena, J. Campo, and Y. Kousaka, "Nucleation, instability, and discontinuous phase transitions in the phase diagram of the monoaxial helimagnet with oblique fields," Phys. Rev. B **95**, 224410 (2017).
[45]Y. Masaki, R. Aoki, Y. Togawa, and Y. Kato, "Chiral solitons in monoaxial chiral magnets in tilted magnetic field," Phys. Rev. B **98**, 100402(R) (2018).
[46]Y. Masaki, "Instabilities in monoaxial chiral magnets under a tilted magnetic field," Phys. Rev. B **101**, 214424 (2020).
[47]V. Laliena, Y. Kato, G. Albalate, and J. Campo, "Thermal fluctuations in the conical state of monoaxial helimagnets," Phys. Rev. B **98**, 144445 (2018).
[48]S. Zhang and Z. Li, "Roles of nonequilibrium conduction electrons on the magnetization dynamics of ferromagnets," Phys. Rev. Lett. **93**, 127204 (2004).
[49]A. Manchon, J. Železný, I. M. Miron, T. Jungwirth, J. Sinova, A. Thiaville, K. Garello, and P. Gambardella, "Current-induced spin-orbit torques in ferromagnetic and antiferromagnetic systems," Rev. Mod. Phys. **91**, 035004 (2019).
[50]A. Hubert and R. Schäfer, *Magnetic Domains* (Springer-Verlag, Berlin/Heidelberg/New York, 2008).
[51]A. Vansteenkiste, J. Leliaert, M. Dvornik, M. Helsen, F. Garcia-Sanchez, and B. V. Waeyenberge, "The design and verification of mumax3," AIP Adv. **4**, 107133 (2014).
[52]J. Leliaert, M. Dvornik, J. Mulkers, J. De Clercq, M. V. Milošević, and B. Van Waeyenberge, "Fast micromagnetic simulations on GPU—Recent advances made with mumax^3," J. Phys D **51**, 123002 (2018).
[53]D. Cortés-Ortuño, M. Beg, V. Nehruji, L. Breth, R. Pepper, T. Kluyver, G. Downing, T. Hesjedal, P. Hatton, T. Lancaster, R. Hertel, O. Hovorka, and H. Fangohr, "Proposal for a micromagnetic standard problem for materials with Dzyaloshinskii–Moriya interaction," New J. Phys. **20**, 113015 (2018).
[54]J. Kishine, K. Inoue, and Y. Yoshida, "Synthesis, structure and magnetic properties of chiral molecule-based magnets," Prog. Theor. Phys. Suppl. **159**, 82–95 (2005).
[55]Y. Togawa, T. Koyama, Y. Nishimori, Y. Matsumoto, S. McVitie, D. McGrouther, R. Stamps, Y. Kousaka, J. Akimitsu, S. Nishihara, K. Inoue, I. G. Bostrem, VI. E. Sinitsyn, A. S. Ovchinnikov, and J. Kishine, "Magnetic soliton confinement and discretization effects arising from macroscopic coherence in a chiral spin soliton lattice," Phys. Rev. B **92**, 220412 (2015).
[56]M. Mito, H. Ohsumi, K. Tsuruta, Y. Kotani, T. Nakamura, Y. Togawa, M. Shinozaki, Y. Kato, J. Kishine, J. Ohe, Y. Kousaka, J. Akimitsu, and K. Inoue, "Geometrical protection of topological magnetic solitons in microprocessed chiral magnets," Phys. Rev. B **97**, 024408 (2018).
[57]S. Tang, R. S. Fishman, S. Okamoto, J. Yi, Q. Zou, M. Fu, A.-P. Li, D. Mandrus, and Z. Gai, "Tuning magnetic soliton phase via dimensional confinement in exfoliated 2D $Cr_{1/3}NbS_2$ thin flakes," Nano Lett. **18**, 4023–4028 (2018).
[58]J. Kishine, I. G. Bostrem, A. S. Ovchinnikov, and V. E. Sinitsyn, "Topological magnetization jumps in a confined chiral soliton lattice," Phys. Rev. B **89**, 014419 (2014).
[59]M. Ohkuma, M. Mito, Y. Kousaka, J. Akimitsu, J. Kishine, and K. Inoue, "Controlling avalanche soliton nucleation in a chiral soliton lattice on a monoaxial chiral magnet $CrNb_3S_6$ by dynamic strain," Appl. Phys. Lett. **118**, 132404 (2021).
[60]K. Koumpouras, A. Bergman, O. Eriksson, and D. Yudin, "A spin dynamics approach to solitonics," Sci. Rep. **6**, 25685 (2016).
[61]S. Rohart and A. Thiaville, "Skyrmion confinement in ultrathin film nanostructures in the presence of Dzyaloshinskii-Moriya interaction," Phys. Rev. B **88**, 184422 (2013).
[62]M. Wilson, E. Karhu, D. Lake, A. Quigley, S. Meynell, A. Bogdanov, H. Fritzsche, U. Rößler, and T. Monchesky, "Discrete helicoidal states in chiral magnetic thin films," Phys. Rev. B **88**, 214420 (2013).
[63]S. Meynell, M. Wilson, H. Fritzsche, A. Bogdanov, and T. Monchesky, "Surface twist instabilities and skyrmion states in chiral ferromagnets," Phys. Rev. B **90**, 014406 (2014).
[64]F. Garcia-Sanchez, P. Borys, A. Vansteenkiste, J.-V. Kim, and R. L. Stamps, "Nonreciprocal spin-wave channeling along textures driven by the Dzyaloshinskii-Moriya interaction," Phys. Rev. B **89**, 224408 (2014).
[65]A. Leonov, Y. Togawa, T. L. Monchesky, A. N. Bogdanov, J. Kishine, Y. Kousaka, M. Miyagawa, T. Koyama, J. Akimitsu, T. S. Koyama, K. Harada, S. Mori, D. McGrouther, R. Lamb, M. Krajnak, S. McVitie, R. L. Stamps, and K. Inoue, "Chiral surface twists and skyrmion stability in nanolayers of cubic helimagnets," Phys. Rev. Lett. **117**, 087202 (2016).
[66]M. Shinozaki, Y. Masaki, R. Aoki, Y. Togawa, and Y. Kato, "Intrinsic hysteresis due to the surface barrier for chiral solitons in monoaxial chiral helimagnets," Phys. Rev. B **97**, 214413 (2018).